The viability of the filler barrier effect during the DC dry-band arcing on silicone rubber

Alqudsi, Alhaytham Y.; Ghunem, Refat A.; David, Éric

Publisher's version / Version de l'éditeur:
https://doi.org/10.1109/TDEI.2022.3198754
IEEE Transactions on Dielectrics and Electrical Insulation, 29, 5, pp. 1873-1881, 2022-08-24

The Viability of the Filler Barrier Effect during the DC Dry-Band Arcing on Silicone Rubber

Alhaytham Y. Alqudsi[1,2], Refat A. Ghunem[2] and Éric David[1]
[1]École de technologie supérieure (ÉTS), Montreal, Canada, H3C 1K3
[2]Metrology Research Center, National Research Council Canada, Ottawa, Canada, K1A 0R6

ABSTRACT

This paper investigates the filler barrier effect on suppressing the erosion of silicone rubber composites during the DC dry-band arcing, by supplementing main micro fillers in silicon rubber, i.e. ground silica and micro-sized alumina tri-hydrate, with fumed silica and nano-sized alumina tri-hydrate fillers. A study framework employing simultaneous thermogravimetric-differential thermal analyses, the inclined plane tracking and erosion test and the dry-arc test is employed. Fumed silica in silicone rubber increases the amount of the crosslinked residue and suppresses silicone rubber depolymerization; whereas nano-sized alumina tri-hydrate releasing water of hydration may adversely impact the residue coherence and promote combustion. The viability of the filler barrier effect is synergistically achieved by adding fumed silica to the main ground silica filler, thereby maintaining the residue integrity. The inclined plane-tracking erosion test confirms the importance of the filler barrier effect of fumed silica in supplementing the volume effect of ground silica in the suppression of the DC dry-band arcing. These filler effects appear to mainly govern the erosion resistance, with insignificant effect shown for thermal conductivity under DC. The dry-arc resistance test is shown as a useful method to simulate a stable dry-band arcing and obtain reproducible surface erosion patterns that correlates with the outcomes of the DC inclined plane tracking and erosion test.

Index Terms — **silicone rubber, DC erosion resistance, DC inclined-plane test, dry-arc resistance test, fumed silica barrier effect.**

1 INTRODUCTION

SILICONE elastomers are commonly utilized as housing materials for outdoor polymeric insulators in electric power distribution and transmission systems. When used in areas of severe pollution, SiR insulators are prone to erosion from dry-band arcing which worsens under the DC as compared to AC voltages [1-3]. Indeed, the stability of the dry-band arcing increases under DC as compared to AC voltages, resulting into a higher amount of heat flux impinging the SiR insulator surface.

Inorganic fillers are incorporated in SiR composites, and the filler's action to enhance the composite thermal conductivity has been highlighted as the main filler action suppressing erosion under AC voltages [4]. The DC erosion resistance of SiR, however, was found to be governed by different actions from thermal conductivity, that rather retard the progress of erosion through the thickness of the composite under the DC dry-band arcing [5]. These actions include the filler volume fraction primarily replacing the depolymerizable SiR content, and an additional action for the filler in creating a barrier shielding the underlying silicone from the dry-band arcing heat [5, 6]. Simply loading the composite with more fillers replaces more of the polymeric fuel for erosion, but achieving filler loading at more than 60wt% becomes a difficult and costly task with conventional fabrication methods. Improving the DC erosion resistance of the composite could therefore be approached by adding nano-sized fillers in order to enhance the filler barrier effect. Limited number of studies have reported a role for the barrier effect of the filler during the dry-band arcing on SiR. Kone *et al.* in [6] examined the role of ground silica residue on SiR erosion during the DC inclined plane tracking and erosion test (DC IPT), and explained how the integrity of the residue shield could be enhanced with larger ground silica filler size. Hosier *et al.* in [7] indicated the impact of the mechanical integrity of the residue structure in SiR on its heat ablation and performance in the IPT. It was found that heavily loaded SiR composites with 50wt% (percent by weight) silica passed the IPT under 4.5 kV_{rms} and the laser ablation test as a result of producing a dense ash layer with coherent mechanical integrity.

The barrier effect of fillers in SiR could be obtained by promoting crosslinking reactions within the silicone polymeric matrix. Guo *et al.* in [8] suggested modulating the crosslinking density of SiR, which enhanced the residue formed during the IPT. In their work, highly crosslinked SiR was found to produce a non-porous silicone oxycarbide ceramic residue at local erosion spots on the SiR surface. Xie *et al.* in [9] incorporated treated silica in addition-curing liquid SiR,

Manuscript received on 11 September 2020, in final form xx Month 20yy, accepted xx Month 20yy. Corresponding author: A. Y. Alqudsi.

concluding that the compact ceramic layer formed during erosion was effective in suppressing the thermal degradation of SiR. Delebecq *et al.* in [10] illustrated that siloxane chain immobilization in SiR is key for ceramizing the SiR residue by producing silicone oxycarbide ceramics in high yield. The incorporation of a platinum catalyst was found to have a significant influence promoting residue ceramization on SiR [8-10].

An earlier study in [11] revealed a significant influence for the fumed silica's interface in tethering the siloxane chains of SiR, thereby suppressing DC erosion in SiR nanocomposites by suppressing depolymerization and promoting a radical-based crosslinking. This interaction was revealed to be more influential in suppressing erosion as compared to the enhancements in the composite thermal conductivity [11]. Investigating the barrier effect of fumed silica on the erosion resistance of SiR has been limited to studying nanocomposites [12], without a clear elucidation being presented on the effect adding other constituent elements that could influence erosion like micro-fillers. Reinforcing micro silica filled SiR with fumed silica to enhance the AC erosion resistance of SiR was investigated in many works such as that in [13]. However, no clear elucidation was presented to highlight the combined volume effect and residue structure characteristics on suppressing erosion, especially under DC. Emphasizing the filler barrier effect associated with fumed silica could only be utilized as a supplementary filler action to the volume of micro-sized fillers replacing the polymeric content fueling erosion.

The addition of commonly used micro-fillers, like ground silica and alumina trihydrate (ATH), in sufficient amounts is an essential requirement for reducing the cost of the outdoor insulators by reducing the silicone content used. In other words, adding fumed silica to micro-filled composites could promote the barrier effect given that the micro-filler is adequately added to enhance the erosion resistance of SiR. In addition, specific sizes of ground silica and the water of hydration released from ATH were shown to promote the formation of harmful residue that could further fuel silicone combustion under the DC IPT [5, 6]. Thus, investigating the viability of the barrier effect associated with supplementing fumed silica and other potential nano fillers, such as nano ATH, to micro-fillers is constrained with ensuring the residue barrier is not adversely impacted by the micro-filler constituents in the SiR composite. As such, this paper investigates the integrity of the barrier effect under the DC dry-band arcing as a result of supplementing fumed silica or nano ATH in SiR composites in the presence of ground silica and ATH as main micro-sized fillers added to the composite.

.

2 MATERIALS AND METHODS

2.1 MATERIAL SPECIMEN

Table 1 describes the fillers and SiR composites used in the study. Both fumed silica and micro ATH fillers were obtained from Sigma-Aldrich. Ground silica and nano ATH were respectively obtained from US Silica and Nanostructured&Amorphous Materials, Inc. The silicone used was a two-part room temperature vulcanized (RTV) SiR from Momentive, RTV 615, in which fillers were added and mixed using a ROSS high shear mixer. The mixer disperses the filler into the base silicone, and later with the crosslinking agent added into the mixture. The procedure followed in preparing the composites can be found in [11].

Five composites were prepared which comprised of micro ATH filled SiR, ground silica filled SiR, and three other hybrid composites combining a micro filler and a nano filler as indicated in Table 1. Practical formulations of SiR should typically contain high silica and ATH micro filler loadings, at least about 40 wt%, in order to pass the critical test voltage of IPT [14, 15] and to which fumed silica could be added to promote a barrier effect [12]. Since only the viability of the filler barrier effect is rather explored here in principle and given the limitation in the laboratory to achieve high loading levels in the composite with nano-sized fillers using the high shear mixer, the total weight fraction of the filler in all composites was maintained at 30wt%. Therefore, this study investigates hybrid composites with micro filler as the main filler replacing the silicone, and a nano filler as the supplementary filler promoting barrier effect respectively in a 25:5 ratio between the micro and nano fillers.

Table 1. Fillers and composites used in the study.

Filler Name	Particle Size (μm)	Specific Gravity
Ground silica	10.5[1]	2.65
Micro ATH	<45	2.42
Fumed silica	7×10^{-3}	2.3
Nano ATH	5×10^{-2} [2]	2.42

Composite Sample Code	Filler Level				Total Filler (wt%)
	Base Filler	Level (wt%)	Supplementary Filler	Level (wt%)	
A30	Micro ATH	30	NA[3]	0	30
S30	Ground silica	30	NA[3]	0	
A25a5	Micro ATH	25	Nano ATH	5	
A25s5	Micro ATH	25	Fumed silica	5	
S25s5	Ground silica	25	Fumed silica	5	

[1]Median particle size. [2]Average particle size. [3]Not applicable.

2.2 THE IPT AND DRY-ARC RESISTANCE TEST

Figure 1 shows the test setup for the IPT and dry-arc resistance test, which conforms to the IEC 60587 and ASTM D495 standards [16, 17]. The test voltage in the IPT, was set to the positive polarity at 3.5 kV level, which produces a severe dry-band arcing that leads to deep erosion on SiR composites [3]. Detailed experimental procedure of the test can be found in [11], which were based on previously recommended procedures for conducting the IPT under +DC voltages (+DC IPT) [3]. Ten samples from each of the composites in Table 1 were tested. After testing was complete, the erosion depth was recorded using a digital Mitutoyo 571-200 micrometer with an accuracy of 0.1 mm. The eroded volume was determined using the weight measured and the known density for a clay material filling the eroded pit.

The dry-arc resistance test was employed in this study as an accelerated testing method for producing a reproducible eroded surface and residue morphology on the tested SiR composites. A low current arc was generated during the test which was utilized as a controlled heat source for controlled heat ablation of SiR. As shown in Figure 1(b), the test uses tungsten electrodes placed at a 30° inclination angle on the sample under test and separated by a distance of 6.35mm. The followed protocol in the test was to generate the low-current arc (scintillation) in seven 1-minute current steps (CS), with specified current magnitude and scintillation duration [17]. Figure 1(b) describes the nature of the current generated during

the first four CSs, CS1 to CS4, of the original seven outlined in [17]. As can be seen in Figure1(b), the scintillation duration increases with the progress of the test which indicates an increase in the degree of stability for the scintillation. The transition from CS3 to CS4 leads to a sustained scintillation. This is analogous to the behavior of the DC dry-band arc evolving into the stable state and imposing more severe heat on the testing surface as compared to intermittent scintillation at early stages of the test [11, 18]. The governing difference between AC and DC dry-band arc comes down to the increased stability of the arc under DC as compared to AC voltages and, thus, there was no need for modifying the existing setup for DC testing. The current magnitude, 10mA, is constant during these four steps and are generated at a 6.1kV AC voltage. The stable arc was obtained by CS4 and thus there was no need to use the entire seven steps outlined in [17]. The coherency and integrity of the damaged surfaces obtained using this test are observed using microscopic tools.

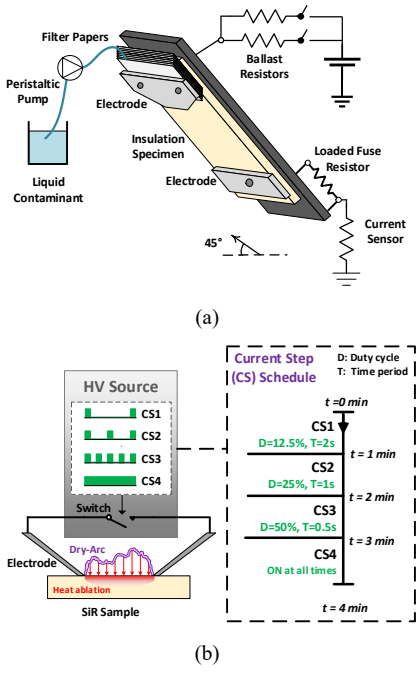

Figure 1. Overall (a) DC Inclined plane tracking and erosion test and (b) dry-arc resistance test setups used in the study.

2.3 THERMAL ANALYSIS

Thermogravimetric-differential thermal analyses (TGA-DTA) were employed in this study to investigate the thermal degradation behavior of the prepared composites. Conducting such analyses is essential for observing the incremental role of the nano filler on suppressing depolymerization and promoting the formation of additional residue promoted by the filler-polymer interactions in the composite. TA instrument's SDT Q600 was used to conduct TGA-DTA under nitrogen (N_2) and air (O_2) atmospheres with an applied heating rate of 25 °C/min and a temperature span between 80-800°C. The tested samples weighed between 10-20 mg. Thermal conductivity measurements were acquired for the composites using a Trident Thermal Conductivity Analyzer which utilizes the Modified Transient Plane Source (MTPS) method as per the ASTM D7984 standard [19].

2.4 RESIDUE MORPHOLOGY

Observing the surface morphology of eroded SiR surfaces is essential in understanding the effect of the fillers in general and nano fillers in particular on altering the SiR residue characteristics in terms of coherency and integrity. Microscopy can characterize the morphology of eroded surfaces based on surface fracture, roughness and porosity. The eroded surfaces of the composites analyzed were obtained through the +DC IPT and the dry-arc resistance test. Scanning electron microscopy (SEM), S3600-N Hitachi, was used in this study to observe the surface morphology of eroded composites under both tests. The samples were prepared by blade cutting, followed by sputter coating with gold. A Keyence VR-5000 optical microscope was also used to scan the surface profiles of the composites in this study. The scanned profiles provide a clear three-dimensional (3D) surface topography that could be used to observe the surface profile in a manner that would facilitate a comparison between the characteristics of the residue structure. This would allow a preliminary observation on whether a barrier-like residue could be obtained in a given composite under erosion.

3 RESULTS AND DISCUSSION

3.1 THERMAL ANALYSIS

Table 2 tabulates the thermal conductivity measurements for the composites of the study. The thermal conductivity measurements obtained for the A30 and S30 are consistent with those obtained in [4]. The addition of 5wt% fumed silica to 25 wt% micro ATH and silica respectively in the A25s5 and S25s5 composites had a significant effect on reducing the thermal conductivity with respect to those measured in A30 and S30 respectively. This, however, was not observed with the addition of nano ATH in A25a5. Khanum *et al.* in [20] explained that the increase in the number of filler-polymer interfaces in SiR composites could obstruct the heat flux and lower the composite thermal conductivity. It could be therefore that the better filler dispersion promoting filler-polymer interfaces with fumed silica as compared to nano ATH lead to the more remarkable decrease in the thermal conductivity with fumed silica as compared to nano ATH. In addition, an earlier study in [11] indicated that the silanol groups on the silica surface had an influential role in promoting favorable interactions with the siloxane chains in SiR. This interaction, however, was not found to be similarly influenced by nano ATH. Rather, filling nano ATH in SiR at 5wt% resulted in the formation of agglomerates in the micron-sized range [11]. The agglomerates could be equivalent in size to the micro ATH filler particles used in A25a5 and thus resulted in no effective change in the thermal conductive pathways as compared to A30.

Table 2. SiR composites thermal conductivity measurements.

Composite Code	Measurement Statistics of thermal conductivity			
	Number of Measurements	Minimum	Maximum	Average
		W/m.K		
S30	15	0.411	0.432	0.420
A30		0.473	0.523	0.495
A25a5		0.474	0.487	0.481
A25s5		0.332	0.371	0.344
S25s5		0.310	0.358	0.332

Figure 2 shows the TGA, DTGA (differential TGA) and DTA plots conducted for the composites of the study under N_2 atmosphere. As per the plots of Figure 2(a), the initial decomposition temperature for the composites were dependent on the type of filler being used in the composite. Composites containing an ATH filler component, A30, A25a5 and A25s5, begin their weight loss near 200 °C, which represents the onset of endothermic dehydration of the micro ATH filler as it was similarly shown in [5, 15] for micro ATH filled SiR composites. At the end of the endothermic dehydration step shown in Figure 2(a) at about 350 °C, a higher remaining weight percentage can be observed for A25s5 and A25a5 as compared to A30.

It is important to note that the amount of depolymerized SiR in the 200 °C - 350 °C temperature range was shown to be insignificant, and therefore the difference in the percentage weight loss remaining at 350 °C, as shown in Figure 2(a), can be primarily attributed to corresponding differences in the amount of the water of hydration released amongst composites. This was similarly reflected in the DTGA plot of Figure 2(b) indicating a higher decomposition rate for A30 as compared to A25a5 and A25s5 composites during the dehydration. An increase in the depth of the corresponding endothermic dent of ATH dehydration is also evident for A30 as compared to A25s5 and A25a5 composites in Figure 2(c). For A25s5, the higher remaining weight percentage at 350 °C was as expected, as a result of the lower weight fraction of the ATH filler releasing water of hydration which is lower in A25s5 as compared to A30 (by 5wt%).

For A25a5, higher remaining weight percentage at 350 °C was also obtained indicating less water of hydration amount released as compared to A30, despite the same total loading level of ATH filler (30 wt%) in A25a5 and A30. It should be noted however that A30 included higher amount of micro ATH as compared to A25a5 (by 5wt%). Therefore, the nano ATH component in A25a5 does not seem to undergo endothermic decomposition in the same manner as compared to the micro ATH during the TGA-DTA. The equal amounts of final residue obtained near 800 °C for the A25a5 and A30 composites suggest the possibility that, with similar total amount of ATH at 30 wt% loaded, similar amount of water of hydration can be released, but the dehydration of the nano ATH component is more distributed during the entire temperature span of the test than micro ATH.

The decomposition stage starting at 400 °C in Figure 2 for the composites represents the beginning of SiR depolymerization as a result of the bond scission of Si-O bonds in the siloxane chains of SiR as reported by Camino *et al.* in [21]. Depolymerization of SiR entails the formation of cyclic oligomers that depart the composite in the form of gaseous volatiles. Hamadani explained that the depolymerization and volatilization of SiR is governed by the mobility and flexibility of the siloxane chains [22]. Delebecq *et al*. in [10] illustrated that the weakly retained portions of the siloxanes chains are prone to depolymerization and volatilization between 400 °C and 640 °C. The constrained mobility of SiR during this decomposition step is highly influenced by the physical interactions between the filler surface and the polymer through hydrogen bonds.

Figure 2(b) indicates the presence of additional decomposition peaks for all the composites beyond 600 °C. This suggests the presence of a competing mechanism with depolymerization during the decomposition of SiR, which is radical-based crosslinking [5-6, 21]. Radical-based crosslinking is explained to be initiated through the homolytic scission of Si-CH_3 bonds at elevated temperatures. During this crosslinking step, the siloxane chains become further restrained and depolymerization is inhibited to finally produce a ceramized residue [22]. Kumagai *et al* described the nature of this ceramized residue to be composed of a semiconductive silicon oxycarbide material [23].

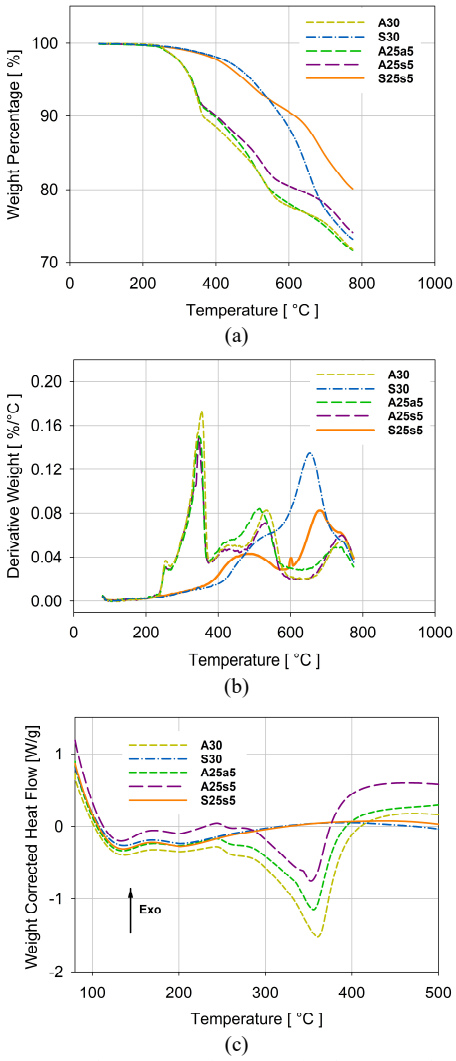

Figure 2. (a) TGA, (b) DTGA and (c) DTA for the prepared composites of the study under N_2 atmosphere.

Comparatively analyzing the thermal decomposition characteristics amongst the composites under TGA is essential for understanding the filler effect during the depolymerization and crosslinking steps exhibited by the composites. Merely using the actual final TGA residue weight (W_{TGA}) from Figure 2(a) as a parameter for such analysis would be impractical, especially in the case of hybrid composites. Accordingly a different approach is adapted in this study which calculates the amount additional residue (W_{add}) formed in the composite during TGA; this approach was also adapted in [6, 12, 24]. The W_{add} estimates the amount of additional crosslinked residue formed as a result of the filler-polymer interactions, by subtracting the assumed TGA residue weight (W_{TGAasu}) from the actual W_{TGA} measured in Figure 2(a). The W_{TGAasu} accounts

for the total sum of alumina and silica filler residue and the undepolymerizable (crosslinked) SiR residue (W_{SiR}).

The W_{SiR} has already been found to be around 14.5wt%, which is the final remnant TGA residue found in unfilled RTV SiR under N_2 atmosphere. The alumina residue is determined by multiplying the ATH weight fraction (W_{ATH}) with a factor of 0.65 which accounts for the 35wt% water content released from the hydrated filler during the TGA [5]. The silica filler does not decompose during the TGA and therefore the silica residue amount is the same as the silica weight fraction (W_{silica}) in the composite. Thus W_{TGAasu} is calculated using (1), and then is used for the calculation of W_{add} in (2).

$$W_{TGAasu} = (0.65 \times W_{ATH}) + (W_{silica}) + (0.145 \times W_{SiR}) \quad (1)$$

$$W_{add} = W_{TGA} - W_{TGAasu} \quad (2)$$

To further understand the impact of the incorporated fillers on suppressing depolymerization, the depolymerized SiR content (W_{dep}) leaving the composite in the form of combustible cyclic oligomer volatiles is calculated. The W_{dep} represents the difference between the amount of SiR content that was available in the composite prior depolymerization, and the amount of additional residue formed at the end of the TGA. Accordingly W_{dep} is calculated using (3).

$$W_{dep} = W_{SiR} - W_{add} \quad (3)$$

Table 3 shows the calculated amounts for W_{add} and W_{dep} for each of the composites at the end of the TGA. According to Table 3, S30 had the least amount of additional residue produced during TGA. This finding confirms that the main filler action of micro silica in SiR is to replace the polymeric fuel of erosion and improve the composite thermal conductivity [4, 6]. Table 3 shows a significant increase in W_{add} as a result of adding fumed silica. This improvement could be attributed to the role of the fumed silica filler in restricting the mobility of the siloxane chains which was otherwise unconstrained with only ground silica added. It was emphasized in [10] that the physical adsorption of the siloxane chains on the fumed silica surface is a key element in promoting large crosslinking during TGA, which could further be enhanced via a radical platinum catalyst. Therefore, reinforcing the micro silica composite with supplementary amount of fumed silica could add a crosslinked residue on the surface during dry-band arcing.

The A30 and A25a5 had equivalent amounts of additional residue produced during TGA which basically indicates no significant influence for the nano ATH filler to alter the thermal degradation mechanisms when added as a supplementary filler in SiR filled with micro ATH as the main micro filler. The addition of fumed silica to micro ATH as the main micro filler in A25s5 had a slight effect on improving the additional residue, but not to a similar extent as when the main micro filler was ground silica. This finding suggests a synergistic effect for a supplementary amount of fumed silica when added with ground silica to silicone rubber in promoting the crosslinked residue during the dry-band arcing. This synergy to promote crosslinking was not observed when adding a supplementary amount of fumed silica to ATH. Therefore, promoting crosslinking is constrained with the synergistic effect of the added supplementary fumed silica filler to the main micro filler in SiR, which is dependent on the type of the base filler used.

Table 3. Calculation of the additional residue and depolymerized SiR amounts under thermogravimetric analysis (TGA).

Composite Code	Filler component weights			Final TGA weight		Additional Residue (W_{add})	Depolymerized SiR (W_{dep})
	W_{silica}	W_{ATH}	W_{SiR}	Assumed (W_{TGAasu})	Actual (W_{TGA})		
	[%]						
S30	30	-	70	40.2	73.2	**33.1**	**37.0**
A30	-	30		29.7	71.7	**42.1**	**28.0**
A25a5	-	30		29.7	71.6	**42.0**	**28.1**
A25s5	5	25		31.4	74.1	**42.7**	**27.3**
S25s5	30	-		40.2	80.1	**40.0**	**30.1**

The calculated amounts for W_{dep} in Table 3 reflect a higher amount of depolymerized SiR content leaving the S30 as combustible oligomers, when compared to the other composites. Figure 3 shows the DTA performed for the prepared SiR composites under air atmosphere. An exothermic hump is observed for all composites indicating the combustion of volatile oligomers produced during depolymerization. The area under the hump represents the amount of enthalpy change during the TGA run, indicating the relative amount by which each composite combusts during depolymerization. As can be evidently seen in Figure 3, the area under S25s5 curve is the smallest compared to the other composites indicating the lowest levels of combustion exhibited by the composite during TGA.

The exothermic peaks in Figure 3 show comparable combustion levels with S30, A30, A25a5. These comparable combustions levels were obtained, despite a much higher depolymerized content fueling combustion as determined in Table 3 with S30. This finding primarily indicates that the additional residue in the ATH filled composites did not inhibit combustion to a similar extent in the ATH-free composites. Rather the level of combustion seems to have been adversely effected with ATH added to the composite. Ghunem *et al.* in [5] illustrated the effect of ATH dehydration in filled SiR composites on the residue structure porosity and roughness. The porosity of the residue structure impacted oxygen diffusion and the consequent level of combustion in the composites under DTA. The weakness of such residue may diminish the possibility of creating a barrier effect for shielding the material during dry-band arcing. Thus, despite the additional residues obtained for A30, A25a5 and A25s5, the residue structure integrity would still need to be verified in order to prevent combustion failure.

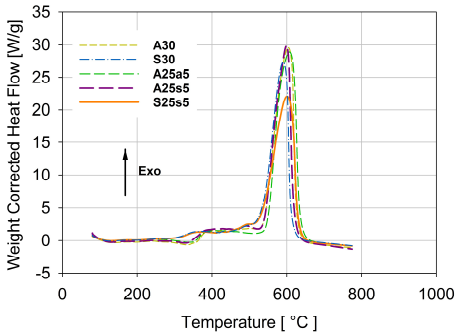

Figure 3. DTA for the prepared composites in air, O_2, atmosphere.

3.2 DC INCLINED PLANE-TRACKING EROSION TEST OUTCOMES

Figure 4 and Figure 5 show the +DC IPT outcomes for the composites of the study. As can be depicted in the post-tested

sample images shown in Figure 4, a variation can be observed within the composites in the extent of damage caused by erosion under DC dry-band arcing. Figure 5 illustrates the erosion depth and eroded volume quantities measured for the composites of the study.

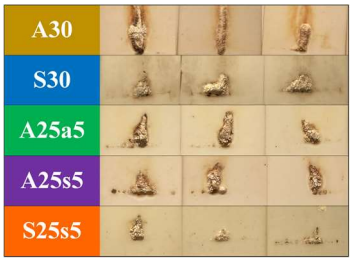

Figure 4. Images for the post-tested +DC IPT specimen samples.

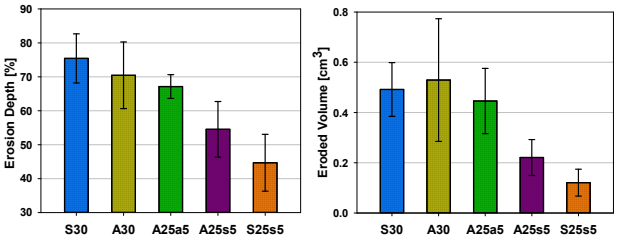

(a) (b)

Figure 5. (a) Erosion depth measurements for the tested composites as percentage of original sample thickness, with the average value and measured values within one standard deviation. (b) Eroded volume for the tested composites with the average value and values measured within one standard deviation.

The outcomes of Figure 5 suggest a superior +DC erosion resistance for the S25s5 composite as compared to the others. It is also important to note that this superior DC erosion resistance was obtained despite S25s5 having the least thermal conductivity measured as shown in Table 2. This highlights that thermal conductivity becomes a less important factor to consider in enhancing the DC as compared to the AC erosion resistance of silicone rubber with fillers [11]. The S30 composite had a much inferior erosion resistance as compared to S25s5 which clearly illustrates the effectiveness in supplementing ground silica with fumed silica to suppress DC erosion. These findings suggest that the synergistic role shown in TGA-DTA for the supplementary fumed silica, added to the micro silica in promoting a crosslinked residue barrier, is important to suppress the progression of erosion during the DC IPT.

The A30 and A25a5 were also among the composites with the worst erosion resistance outcomes under the +DC IPT, despite having the highest measured thermal conductivities. Figure 3 did indicate the highest combustion observed during depolymerization for these composites under air atmosphere. The A25s5 composite containing fumed silica seems to have a relatively better erosion resistance compared to S30, A30 and A25a5. In addition, the S25s5 surpasses all the composites in terms of the erosion resistance obtained and showed least amount of combustion in the DTA shown in Figure 3. These findings highlight the role of the fumed silica in constraining the mobility of the siloxane chains, which suppressed depolymerization and promoted crosslinking in the composite. These findings also emphasize on the synergistic effect in adding the fumed silica to ground silica in prompting a better shield in retarding combustion and thus improving the erosion resistance of silicone rubber.

3.3 THE DRY-ARC RESISTANCE TEST

Figure 6 shows the 3D surface topography obtained for the tested composites under the dry-arc resistance test. The generated topography shows a variation amongst the composites in terms of the coherency and roughness of surfaces. A clear difference can be seen between the S25s5 composite surface as compared to all the other composites. The produced surface residue seems to be more intact and coherent as compared to the others. Insignificant difference in the residue morphology can be observed for eroded surfaces obtained for the A30, S30 and A25a5 with the surfaces being highly rough and incoherent. The addition of fumed silica to micro ATH in A25s5 somewhat shaped the residue towards a more coherent structure, but not as was synergistically obtained when fumed silica was added to ground silica in silicone rubber.

Ranking the order of the tested composites in terms of increasing structure coherency would result in having the S25s5 eroded surface being of superior coherency compared to all the other composites, followed by the A25s5 surface residue being somewhat more coherent as compared to the remaining composites. This ranking seems to support the correlation suggested between the +DC IPT outcomes reported in Figure 5 and the role of the filler barrier effect during the dry-band arcing. The coherency in the residue structure defines the filler barrier effect as an incremental mechanism to the volume effect of the filler in hindering progressive erosion in the composites.

This clarity in observing the residue structures was possible as a result of the dry-arc resistance test protocol facilitating obtaining reproducible erosion surface patterns due to a controlled scintillation activity on the surface [24]. The laser ablation method was utilized as an accelerated testing method for ranking the erosion resistance of SiR composites in [25] and as means to observe the integrity of the produced residue in various insulating materials [7]. The dry-arc resistance test, however, utilizes stable scintillations during the test in a manner similar to that of the DC dry-band arcing in the IPT, which makes it more practical for the purpose of this study.

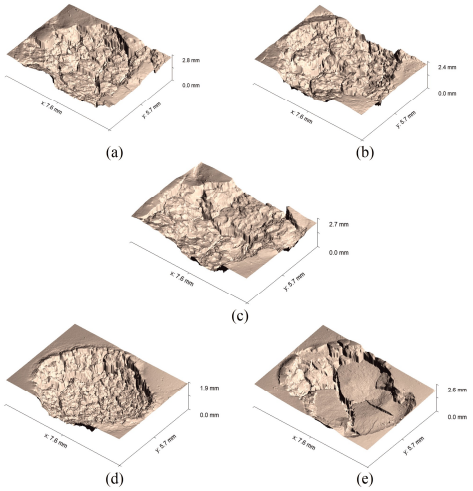

Figure 6. 3D surface topography for the post-tested samples of (a) A30, (b) A25a5, (c) A25s5, (d) S30, and (e) S25s5 under the dry-arc resistance test.

Figure 7 shows the SEM images obtained for the eroded surfaces of the composites under the +DC IPT and dry-arc resistance test. The images for a given composite under both tests correlate in terms of the surface roughness and coherency. This validates the approach proposed in this study in using the dry-arc resistance test as means for accelerating the erosion of the composites in a manner similar to that exhibited in the +DC IPT to observe the residue structure characteristics as was similarly done in [24]. The eroded residue obtained for S25s5 under both tests was found to be coherent and nonporous as compared to the other composites. The eroded surfaces of S30, A30 and A25a5 were found to be much more incoherent and rougher under both tests. The surface of A25s5 was found to have slight improvements in the residue structure and integrity. The residue structure characteristics observed with SEM under both tests support explaining the impact of the residue integrity on the DC erosion resistance of the composites.

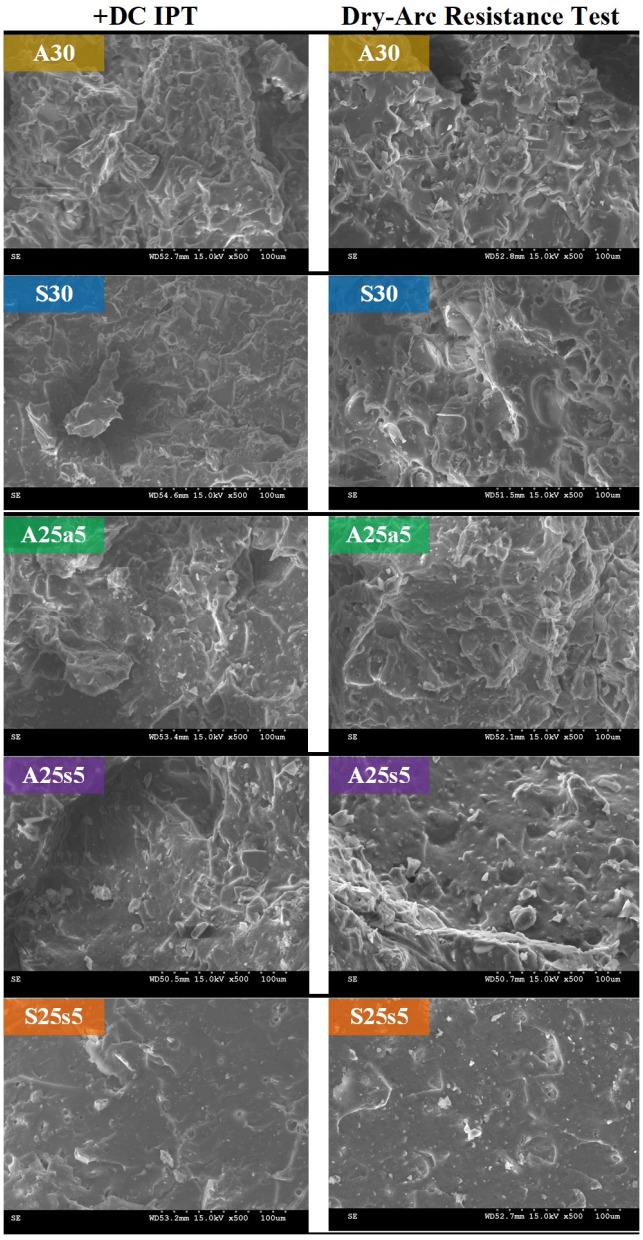

Figure 7. SEM imaging for the eroded surfaces under a magnification of x500 for the composites tested under the +DC IPT and dry-arc resistance test.

CONCLUSION

This paper investigates the viability of the filler barrier effect shielding SiR composites during DC dry-band arcing. A testing framework employing the TGA-DTA, the IPT and the dry-arc test is introduced. Outcomes indicate a significant influence for fumed silica in promoting a crosslinked residue during the dry-band arcing as compared to nano ATH, which was primarily attributed to the favorable interactions between fumed silica and SiR. In addition, a synergistic effect for adding fumed silica to ground silica in SiR is shown which resulted in a remarkably coherent residue, leading to suppression of combustion and thus an enhanced erosion resistance under DC voltage. Therefore, the barrier effect which is characterized with the coherency and integrity of the residue structure should be an additional important factor to be considered with the volume effect of the filler to design silicone rubber composites for DC outdoor insulation applications. The thermal conductivity on the other hand is not shown to be a governing parameter on the DC erosion resistance of the composites. The dry-arc test is shown as a useful tool simulating the stable dry-band arcing and resulting in reproducible erosion outcomes on silicone rubber that correlate with the DC IPT outcomes.

ACKNOWLEDGEMENT

The authors gratefully acknowledge the Natural Sciences and Engineering Research of Canada (NSERC) for the financial support. The authors would like thank to Dr. Souheil-Antoine Tahan, Mr. Simon Laflamme, Dr. Mohammad Saadati and Mr. Joel Grignon for providing the technical help needed for the microscopic work in this paper.

REFERENCES

[1] X. Liang *et al*, "Improving the outdoor insulation performance of Chinese EHV and UHV AC and DC overhead transmission lines," IEEE. Electr. Insul. Mag., vol. 36, no. 4, pp. 7-25, Jul.−Aug. 2020.

[2] J. V. Vas, B. Venkatesulu and M. J. Thomas, "Tracking and erosion of silicone rubber nanocomposites under DC voltages of both polarities," IEEE. Trans. Dielectr. Electr. Insul., vol. 19, no. 1, pp. 91-98, Feb. 2012.

[3] E. A. Cherney *et al*, "DC inclined-plane tracking and erosion test of insulating materials," IEEE. Trans. Dielectr. Electr. Insul., vol. 22, no. 1, pp. 211-217, Feb. 2015.

[4] L. H. Meyer, E. A. Cherney and S. H. Jayaram, "The role of inorganic fillers in silicone rubber for outdoor insulation alumina tri-hydrate or silica," IEEE. Electr. Insul. Mag., vol. 20, no. 4, pp. 13-21, Jul.-Aug. 2004.

[5] R. A. Ghunem *et al*, "Effect of hydrated fillers in silicone rubber composites during AC and DC dry-band arcing," IEEE. Trans. Dielectr. Electr. Insul., vol. 27, no. 1, pp. 249-256, Feb. 2020.

[6] D. Koné *et al*, "Effect of residue formed during the AC and DC dry-band arcing on silicone rubber filled with natural silica," IEEE. Trans. Dielectr. Electr. Insul., vol. 26, no. 5, pp. 1620-1626, Oct. 2019.

[7] I. L. Hosier *et al*, "Comparison of laser ablation and inclined plane tracking tests as a means to rank materials for outdoor HV insulators," IEEE. Trans. Dielectr. Electr. Insul., vol. 20, no. 5, pp. 1808-1819, Oct. 2013.

[8] Y. Guo *et al*, "Enhancement of tracking and erosion resistance of silicone rubber with platinum/amino-silane by modulation of crosslinking density IEEE. Trans. Dielectr. Electr. Insul., vol. 25, no. 2, pp. 741-748, Apr. 2018.

[9] C. Xie *et al*, "Remarkable enhancement of tracking resistance of addition-cure liquid silicone rubber by alkyl-disubstituted ureido siloxane immobilized on the silica filler surface," Polym. Degrad. and Stabil., vol. 188, no. 109565, Jun. 2021.

[10] E. Delebecq *et al*, "High Residue Contents Indebted by Platinum and Silica Synergistic Action During the Pyrolysis of Silicone Formulations," ACS Appl. Mater. Interfaces, vol. 3, no. 3, pp. 869–880, Mar. 2011.

[11] A. Y. Alqudsi, R. A. Ghunem and É. David, "Analyzing the Role of Filler Interface on the Erosion Performance of Filled RTV Silicone Rubber under

DC Dry-band Arcing," IEEE. Trans. Dielectr. Electr. Insul., vol. 28, no. 3, pp. 788-796, Jun. 2021.
[12] A. H. El-Hag *et al*, "Erosion resistance of nano-filled silicone rubber," IEEE. Trans. Dielectr. Electr. Insul., vol. 13, no. 1, pp. 122-128, Feb. 2006.
[13] I. Ramirez, S. Jarayam and E. A. Cherney, "Performance of silicone rubber nanocomposites in salt-fog, inclined plane, and laser ablation tests," IEEE. Trans. Dielectr. Electr. Insul., vol. 17, no. 1, pp. 206-213, Feb. 2010.
[14] S. Ansorge, F. Schmuck and K. O. Papailiou, "Improved silicone rubbers for the use as housing material in composite insulators," IEEE. Trans. Dielectr. Electr. Insul., vol. 19, no. 1, pp. 209-217, Feb. 2012.
[15] S. Kumagai and N. Yoshimura, "Tracking and erosion of HTV silicone rubber and suppression mechanism of ATH," IEEE. Trans. Dielectr. Electr. Insul., vol. 8, no. 2, pp. 203-211, Apr. 2001.
[16] Electrical Insulating Materials Used Under Severe Ambient Conditions - Test Methods for Evaluating Resistance to Tracking and Erosion, IEC 60587 2007-05.
[17] Standard Test Method for High-Voltage, Low-Current, Dry Arc Resistance of Solid Electrical Insulation, ASTM D 495-14.
[18] R. A. Ghunem S. H. Jayaram and E. A. Cherney, "Investigation into the eroding dry-band arcing of filled silicone rubber under DC using wavelet-based multiresolution analysis," IEEE. Trans. Dielectr. Electr. Insul., vol. 21, no. 2, pp. 713-720, Apr. 2014.
[19] Standard Test Method for Measurement of Thermal Effusivity of Fabrics Using a Modified Transient Plane Source (MTPS) Instrument, ASTM D7984-16.
[20] K. K. Khanum, R. Ghunem and A. El-Hag, "Thermal Characteristics of Various Silicone Rubber Composites Filled with Silica," *Ann. Conf. Electr. Insul. and Dielect. Phenom. (CEIDP)*, 2020, pp. 31-34.
[21] G. Camino, S.M Lomakin and M. Lageard, "Thermal polydimethylsiloxane degradation. Part 2. The degradation mechanisms," Polym., vol 43, no.7, pp. 2011-2015, Mar. 2002.
[22] S. Hamdani *et al*, "Flame retardancy of silicone-based materials," in Polym. Degrad. and Stabil., vol. 94, no. 4, pp. 465-495, Apr. 2009.
[23] S. Kumagai, X. Wang and N. Yoshimura, "Solid residue formation of RTV silicone rubber due to dry-band arcing and thermal decomposition," IEEE. Trans. Dielectr. Electr. Insul., vol. 5, no. 2, pp. 281-289, Apr. 1998.
[24] A. Y. Alqudsi, R. A. Ghunem and E. David, " A Novel Framework to Study the Role of Ground and Fumed Silica Fillers in Suppressing DC Erosion of Silicone Rubber Outdoor Insulation," Energies, vol. 14, no. 12-3449, Jun. 2021.
[25] L. H. Meyer, S. H. Jayaram and E. A. Cherney, "A novel technique to evaluate the erosion resistance of silicone rubber composites for high voltage outdoor insulation using infrared laser erosion," IEEE. Trans. Dielectr. Electr. Insul., vol. 12, no. 6, pp. 1201-1208, Dec. 2005.

Alhaytham Alqudsi (M'09) received the B.Sc. and M.Sc. degrees in electrical engineering from the American University of Sharjah, Sharjah, UAE, in 2011 and 2016, and a M.S. degree in electrical and computer engineering from Worcester Polytechnic Institute, Worcester, MA, USA in 2019. Alhaytham is pursuing a PhD degree in Engineering at École de technologie supérieure in Montreal, Canada. Moreover, he is a member of the of the NRC Metrology Research Center at the National Research Council Canada, Ottawa, Canada. His research interests include outdoor insulation, machine learning, RF sub-systems, and renewable energy.

Refat Atef Ghunem (M'11-SM'15) received the B.Sc. and M.Sc. degrees from the American University of Sharjah, UAE, in 2008 and 2010, respectively, and the Ph.D. degree from the University of Waterloo in 2014. Dr. Ghunem is a Research Officer with the NRC Metrology Research Center at the National Research Council Canada. Refat is a professeur associé in the Ecole de technologie supérieure, an associate editor for the IEEE Transactions on Dielectrics and Electrical Insulation, the Chair of the IEEE outdoor insulation technical committee of the IEEE Dielectrics and Electrical Insulation Society and a registered professional engineer in the province of Ontario. Dr. Ghunem chaired the working group on the IEEE Std.1523-2018, "IEEE Guide for the Application, Maintenance, and Evaluation of Room-Temperature Vulcanizing (RTV) Silicone Rubber Coatings for Outdoor Ceramic Insulators" and is currently chairing the IEEE working group on IEEE Guide for DC Inclined Plane Tracking and Erosion Test for Outdoor Insulation Applications. His research interests include outdoor insulation, application of novel measurement techniques in the study of polymeric insulating materials and high accuracy electrical power measurements

Éric David (M'03-SM'07) was born in Montreal in 1965. He received the M.Sc.A and Ph.D. degrees in engineering physics from the Ecole Polytechnique de Montréal in 1989 and 1996, respectively. He joined the 'Hydro-Québec Research Institute in 1998, and from 2001 to 2002, where he was active in the field of dielectric materials used for underground cables and rotating machines. He is now a Professor at the Department of Mechanical Engineering in the Ecole de Technologie Supérieure in Montreal. His research interests include dielectric and nanodielectric materials, rotating machinery and underground cable insulation. He is an Associate Editor of the IEEE Transactions on Dielectrics and Electrical Insulation.